Grain Topography in Perpendicular Thin-Film Media and Impact of Possible Surface Anisotropy

Jian-Gang Zhu[1], *Fellow, IEEE*, Hua Yuan[1], Soyoung Park[1], Thomas Nuhfer[2], and David E. Laughlin[1]

[1]Data Storage Systems Center, Carnegie Mellon University, Pittsburgh, PA 15213 USA
[2]Department of Materials Science and Engineering, Carnegie Mellon University, Pittsburgh, PA 15213 USA

In this paper, we present a combined transmission electron microscopy study and micromagnetic modeling investigation of current granular-continuous-composite (CGC) perpendicular thin-film media. Our transmission electron microscopy-EELS elemental analysis on CoCrPt-TiOx layers found evident Cr segregation to the grain boundaries as well as in the middle of a grain where Co and Pt appears to be deficient. Similar localized Co and Pt deficiency is also found in CoCrPt-SiOx media, however, Cr segregation is much less evident. STEM-HAADF analysis reveals that the apparent non-uniform composition is the result of a "cavity-like" topography of the magnetic grains. It is argued that the "cavity" grain topography significantly enhances the grain boundary surface area. Micromagnetic modeling investigation was conducted to study the impact of possible surface anisotropy to the corresponding grain switching field. A systematic numerical analysis is presented.

Index Terms—**Perpendicular recording media, surface anisotropy, switching field, thin-film media.**

I. Introduction

SWITCHING field distribution in perpendicular thin-film media is an important property parameter affecting transition noise, especially at high linear densities. Understanding the correlation between film microstructure and grain switching field distribution is thus critical to the media optimization for continuing increase of area density capability [1]–[4].

An important factor that has been seldom mentioned in literature is the impact of possible grain boundary surface anisotropy. Extensive experimental and theoretical research over the past have shown that the surface of transition metals often exhibit strong magnetic anisotropy with its easy axis perpendicular to the surface and with strong dependence on the interfacial material and interfacial properties [5], [6]. For the current perpendicular thin-film media used in hard disk drive products, the magnetic storage layer comprises a layer of CoCrPt grains with well defined oxide grain boundaries [7]–[10]. Reduction of the grain size increases the grain boundary surface to grain volume ratio. The influence of grain boundary surface anisotropy therefore can no longer be ignored as grain size continues to decrease as required by the increase of area storage density.

In this paper, we present a transmission electron microscopy study utilizing both EELS (electron energy loss spectroscopy) elemental mapping capability and the STEM HAADF (scanning transmission electron microscopy, high angle annular dark field) imaging technique for high spatial resolution characterization of both composition and topography at the grain level [11]. A combined micromagnetic modeling investigation on the impact of surface anisotropy is also presented.

II. High Resolution Transmission Electron Microscopy Analysis

Perpendicular thin-film medium samples are obtained from current commercial hard disk drive products with area storage density capability of about 250 Gb/in^2. For all the samples that we obtained, the media comprise a CoCrPtB continuous layer on top of a CoCrPt-Oxide granular layer in which the oxide grain boundaries are well defined, as shown in the cross-section transmission electron microscopy micrograph shown in Fig. 1.

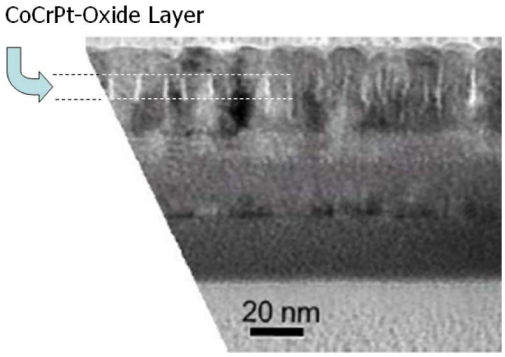

Fig. 1. Cross-section transmission electron microscopy micrograph of a typical perpendicular thin-film medium sample. The CoCrPt layer with oxide grain boundaries shown in the figure is the focus of this study.

In this paper, we focus on the granular magnetic layer with oxide grain boundaries. Careful transmission electron microscopy sample preparation procedure is required for accurate analytical analysis. For the CoPtCr-oxide layer in plan-view samples, the sample was firstly cut in to $\sim 5 \times 5$ mm^2 pieces from the medium disk. It was initially mechanically ground from the substrate back-side using silicon carbide abrasive grinding paper down to $\sim$18 um in thickness. Then, the sample was further back-thinned by ion-milling using a Gatan precision ion polishing system (PIPS) until large areas of the thin layer(s) of interest are electron transparent as illustrated in Fig. 2. By controlling the milling process during sample preparation, i.e., by varying the size of the milled hole and the milling angle, samples with an adequately thinned residual continuous layer and an undamaged granular layer can be produced. Specifically, the thin areas in many little ion-milled holes around the main hole are preferred for much better mechanical stability for the extended electron beam exposure in the analysis. For

Manuscript received November 10, 2008. Current version published February 11, 2009. Corresponding author: J.-G. Zhu (e-mail: jzhu@ece.cmu.edu).

Color versions of one or more of the figures in this paper are available online at http://ieeexplore.ieee.org.

Digital Object Identifier 10.1109/TMAG.2008.2010674

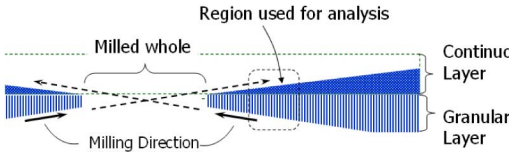

Fig. 2. Illustration of sample preparation for transmission electron microscopy imaging of the magnetic layer with oxide grain boundaries, i.e., the granular layer. By controlling the size of the milling whole and the milling angle, samples with adequate residual thickness of the top continuous layer.

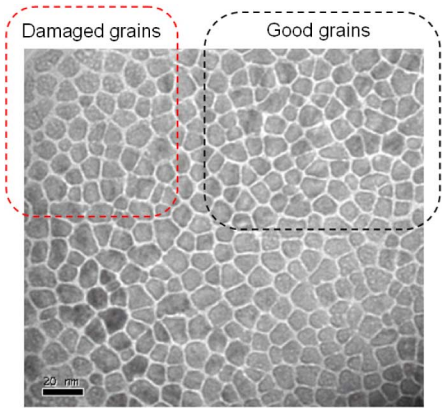

Fig. 3. An example of transmission electron microscopy samples prepared by ion milling. Regions with ion milling damaged grains can be clearly observed.

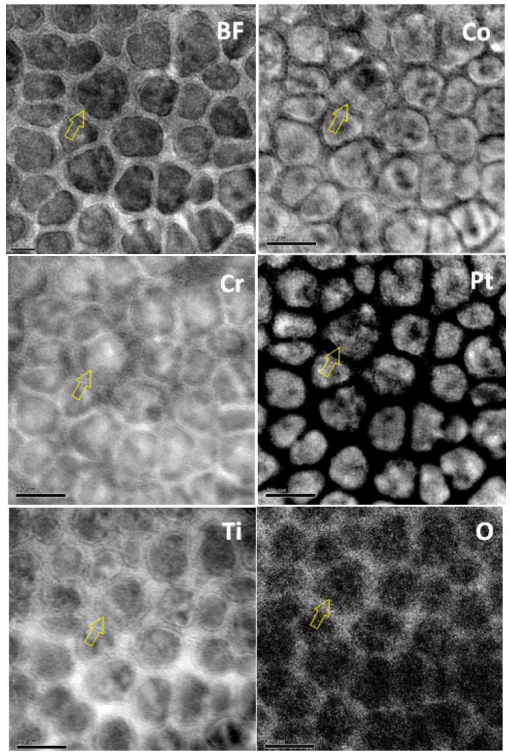

Fig. 4. EELS elemental mapping of all the elements in the granular layer of a CoCrPt-TiOx disk medium sample. The bright field (BF) is included for reference. The scale bar indicates 10 nm dimension.

cross-sectional samples, the sample preparation procedure is more complicated and time-consuming. The resultant good thin area for analytical analysis is much less. Typically, two sample pieces with rectangular shapes were glued together face to face at the film side. The glued stack was cut into pieces with around 1.5 mm in thickness, which was slightly ground on both sides to produce smooth surfaces.

Then, one side was thinned by mechanical grinding to $\sim$40 um. The other side was subsequently dimpled in the same area. The final thickness was reduced to $\sim$20 um. The sample was then ion-milled from both sides.

Here, it is necessary to emphasize that an effort has been made to avoid any ion milling of the magnetic layer with the oxide grain boundaries. Fig. 3 shows a plane view transmission electron microscopy micrograph of a typical transmission electron microscopy sample with regions containing damaged grains and regions with good grains on which transmission electron microscopy imaging was performed. The following aspects were attended to during the imaging and analysis. Firstly, we avoid those damaged thin areas such as 1) the curled and distorted thin area of the samples along the sample hole by electron beam illumination; 2) the drifting thin area during the first 1–2 hours after transmission electron microscopy alignment and sample installation due to long time exposure; 3) the thin area with damaged grains or amorphorized grains by ion-milling processes; 4) the thin re-deposited thin areas by ion milling; and 5) the thin area with abnormally loose packed grains due to over ion-milling processes, etc. In the areas we choose to perform detailed transmission electron microscopy analysis, adequate thickness of the continuous magnetic capping layer has been always maintained to avoid any damage of the interested magnetic layer.

Fig. 4 shows EELS elemental mapping of an CoCrPt-TiOx medium sample for Co, Pt, Cr, Ti and O of the same region. The bright field (BF) image is included for reference. In the elemental mapping images, brighter areas indicate content rich and darker areas indicate content deficiency. The Co mapping shows that Co is essentially absent in grain boundaries. More importantly, almost every grain shows a Co deficient region within the grain interior. Some Co deficient regions have elongated slot-like shapes and some are more or less circular. The Pt mapping shows an evident correlation with the Co mapping: Pt is deficient wherever Co is deficient. In addition, Pt seems to be missing near the grain boundaries since the size of grains in the Pt image is evidently smaller than that shown in both the BF image and the Co mapping image. However, the Cr mapping image shows evident anti-correlation with both the Co and Pt mapping: Cr is enriched at the grain boundaries and also in the grain interiors where Co and Pt are deficient! Both Ti and O are distributed mainly in grain boundaries with little indication of their presence in the interior of the grains.

The exhibited nonuniform composition distribution in the grain interior for Co, Pt, and Cr appears to be a common phenomenon for all the CoCrPt-TiOx disk media samples that we studied. Fig. 5 shows similar transmission electron microscopy images obtained from a different disk drive manufacture, also a CoCrPt-TiOx medium. Similarly, the Co and Pt distributions within grain interiors are correlated: there exists a region or regions within almost every grain where both Co and Pt are deficient. Segregation of Cr to grain boundaries is evident. Also the Cr concentration enhancement within grain interiors where Co and Pt are deficient can still be observed. It should be noted

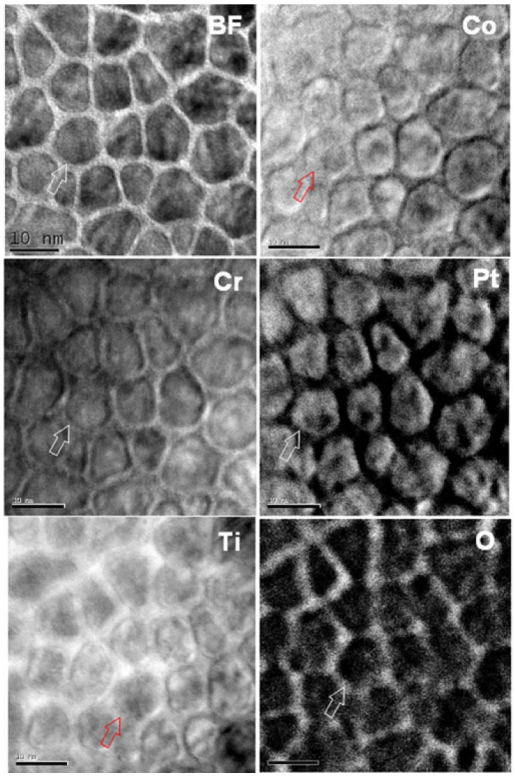

Fig. 5. EELS image of elemental mapping for the elements found in a perpendicular hard disk medium sample. The bar at left bottom indicates 10 nm scale.

here that EELS Pt mapping may not be reliable since its energy peak coincides with a much broader and larger plasmonic resonance peak. We will discuss this later.

Fig. 6 shows a set of cross-section transmission electron microscopy-EELS images on a CoCrPt-TiOx disk medium sample. The deficiency, or absence, of Co in the grain boundaries is evidently through the entire grain thickness. Relatively rich Cr concentration within grain boundaries is also apparent. Ti obviously is present in the grain boundaries also through the entire depth of the layer.

Fig. 7 shows a set of EELS elemental mapping images for a CoCrPt-SiO_x perpendicular disk medium sample. In this case, Co and Pt mappings also show deficient regions in the interior of almost every grain. (Although Pt mapping is not shown here, its distribution closely follows Co.) However, the Co deficient regions in the grain interior appear to be slot-like connecting to grain boundaries, as shown in the figure. The main difference in comparison with the CoCrPt-TiOx samples is the Cr distribution: no obvious composition segregation is observed and its distribution appears to be spatially uniform for the CoCrPt-SiOx sample.

The more pronounced Cr segregation to the grain boundaries in the CoCrPt-TiOx samples relative to that in CoCrPt-SiOx samples suggests that higher perpendicular anisotropy strength may be achieved with TiOx because of the better magnetic grain isolation.

The observed Co and Pt deficiency in the interior of a grain has also been reported in previous publications based on both transmission electron microscopy-EELS and Energy Dispersive analysis of x-rays, EDAX [12]–[14]. In those publications,

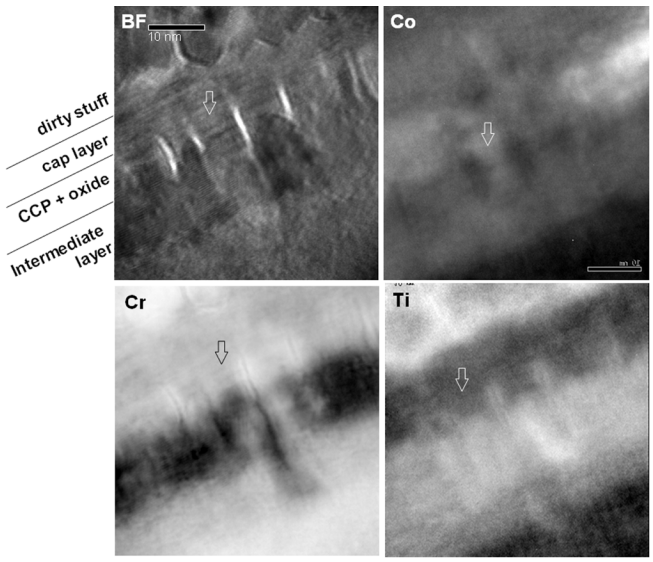

Fig. 6. Cross sectional EELS images for Co, Cr, and Ti of a CoCrPt-TiOx perpendicular disk sample. A bright field (BF) image is included for reference. The arrow in each picture indicates the same location of the sample.

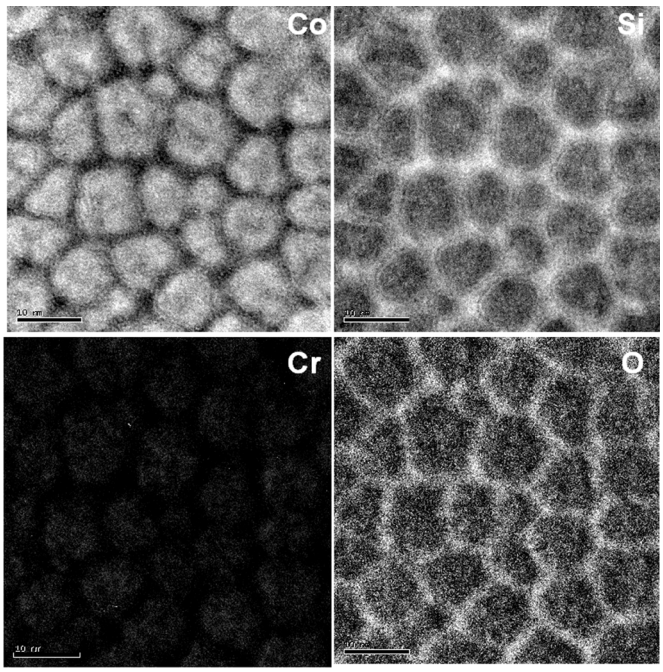

Fig. 7. EELS image of elemental mapping for Co, Si, Cr, and O in a CoCrPt-SiOx perpendicular disk medium sample.

the Co and Pt deficient regions were referred to as "low mass pockets."

To understand the observed composition distribution within a grain, we performed a series additional transmission electron microscopy analysis, utilizing high angle annular dark field (HAADF) imaging technique. Fig. 8 shows a HAADF image with sample surface tilting angle of 36° for the same CoCrPt-SiOx sample used in EELS elemental mapping shown in Fig. 7. The image clearly shows both round and slotted shaped cavities. The detailed comparison between the EELS Co and Pt images

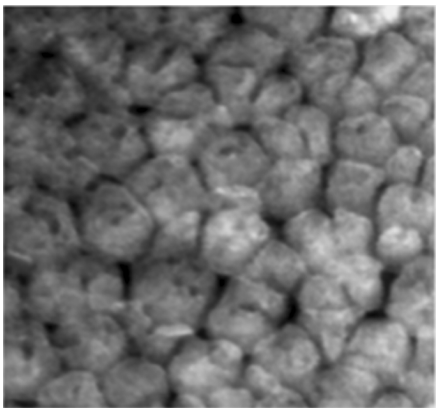

Fig. 8. STEM-HAADF image of a CoCrPt-SiOx sample. The slot-like cavity in the middle of a grain is evident. The perspective view is obtained with a 36° tilting angle of the sample with respect to imaging plane.

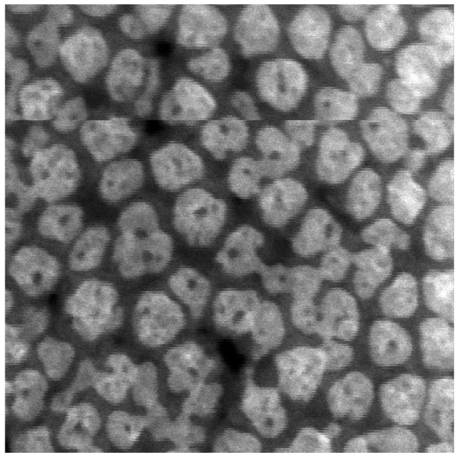

Fig. 9. STEM-HAADF image of a CoCrPt-TiOx sample without sample surface tilting. Both round and slot-shaped cavities of the grains are evident.

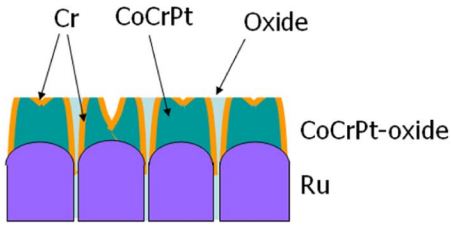

Fig. 10. Illustration of the grain topography interpretated from the presented transmission electron microscopy-EELS and STEM-HAADF analysis on CoCrPt-Oxide perpendicular disk medium samples. The segregation of Cr is much more pronounced in TiOx samples than that in SiOx samples. The oxide appears to be only to form grain boundaries while not appear to be in cavities. The sketched structure is referred to as the tooth structure.

and the HAADF image for the same area show that the Co and Pt deficient regions correspond exactly to the observed cavities.

Now, the observed anticorrelation between the Cr distribution and the Co and Pt distribution in TiOx samples can be understood: Cr not only segregates to the grain boundaries, but also segregates to the inside surfaces of the cavities in the middle, as illustrated in Fig. 10. The fact that no significant oxide is observed in the cavities indicates oxide grain boundaries are formed by template growth, not by elemental segregation.

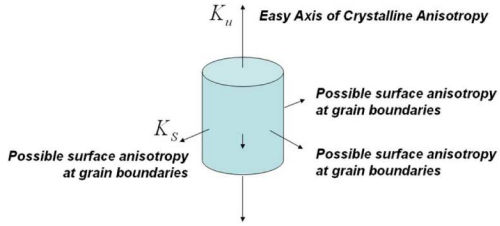

Fig. 11. Illustration of possible surface anisotropy for a grain with bulk perpendicular magnetocrystalline anisotropy.

The sketch shown in Fig. 10 can be naturally referred to as the tooth structure. A similar sketch, although not exactly the same, was also introduced in [15]. One of the mechanisms for forming such teeth structures could be that the material growth along the oxide grain boundaries is relatively faster than the middle of the grains. However, identifying the exact formation mechanism would require significantly more work that is beyond the scope of this paper.

Although the EELS Pt mapping shown in Figs. 4 and 5 may not be reliable, it should not affect the proposed tooth-like grain topography. Since the plasmonic resonance peak can only arise from metallic regions, any plasmonic contribution in the Pt mapping image could be interpreted as metallic mapping. Then, the referred "Pt deficient" region could be interpreted as the region where metallic material is missing. If the oxide material is also missing in the region, the region can only be a void.

III. Micromagnetic Modeling Analysis

Besides the obvious consequence of the teeth structures for causing grain volume reduction, the formation of the cavities could yield a significant increase of inside surface area for a grain. For small size grains, the increase of the surface area can be very significant. Very likely significant magnetic surface anisotropy with easy axis normal to the surface exists for typical Co-alloy grains, a relatively large inside surface area to volume ratio could yield sizable reduction of effective grain anisotropy field as illustrated in Fig. 11.

In this section, we present a micromagnetic modeling analysis for the impact of the tooth structures in the presence of the surface magnetic anisotropy as well as the dependence on grain size. Thus, the effective perpendicular uniaxial anisotropy in the presence of the surface anisotropy can be represented as

$$K_{\text{grain}} = \frac{K_u V - K_S S}{V} = K_u - K_S \left(\frac{S}{V}\right) \qquad (1)$$

where K_u is the bulk uniaxial magnetocrystalline anisotropy energy constant, K_s the surface anisotropy energy constant, S is the side surface area, and V the grain volume.

To model the magnetic switching of a single grain, the grain is divided into a three-dimentional array of 1 nm^3 cubic mesh cells, as illustrated in Fig. 12. The height (i.e., thickness of the granular layer) of the grain is fixed at 14 nm for all the results presented in this section. The bulk crystalline anisotropy energy constant is assumed to be $K = 6 \times 10^6$ erg/cm^3 and the saturation magnetization is assumed to be $Ms = 600$ emu/cm^3. The magnetization within each mesh cell is assumed to be uniform

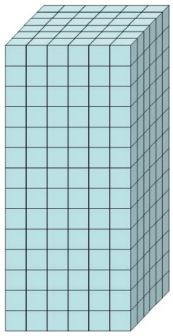

Fig. 12. Illustration of a solid meshed magnetic grains.

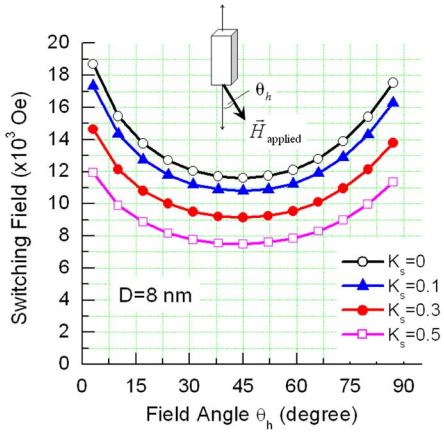

Fig. 13. Calculated magnetic switching field of a solid grain as function of field angle for various surface anisotropy strength. The grain size (side dimension) is $D = 8$ nm and the unit for various Ks values is erg/cm^3.

and its orientation is determined by solving the set of coupled Landau-Lifshitz-Gilbert equations with a Gilbert damping constant $\alpha = 0.1$. The effective magnetic anisotropy is calculated by applying (1), at a mesh cell level. A cavity or a cylindrical whole within a grain is created by taking out the corresponding mesh cells. Since we are going to focus only on the effect of surface anisotropy, the thermally excited magnetization process is purposely neglected.

Fig. 13 shows calculated magnetic switching field of a solid grain as a function of the applied field angle with respect to the perpendicular direction for various surface anisotropy strengths. For a solid grain, increasing the surface anisotropy strength yields a reduction of the switching field while the dependence on the field angle remains virtually unchanged. At a field angle of 10°, the calculated switching field reduction is linearly dependent on the surface anisotropy strength, the same as (1).

With surface anisotropy, the increase of surface to volume ratio as grain size decreases results in a size dependence for the switching field. Fig. 15 shows the calculated switching field as a function of grain size for different surface anisotropy strengths. In the absence of surface anisotropy and thermal excitation, the switching field is virtually independent of the grain diameter. The presence of significant surface anisotropy causes the switching field to decrease with decreasing grain diameter.

Since a void or hole in the middle of a grain increases the inside surface area, the switching field will certainly be reduced in

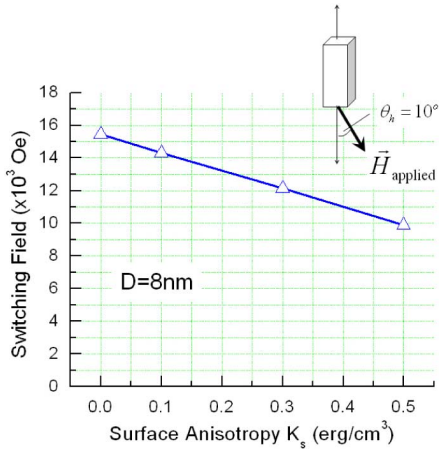

Fig. 14. Calculated switching field as a function of surface anisotropy strength at a fixed applied field angle.

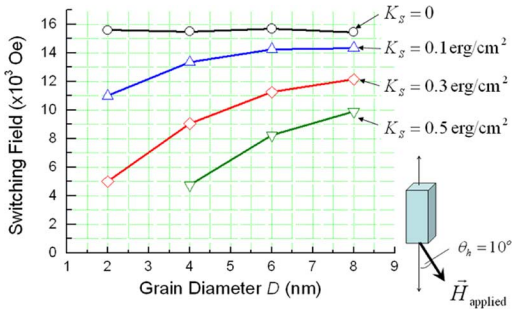

Fig. 15. Calculated switching field as a function of grain diameter for various surface anisotropy strengths. The field is applied at an angle of 10° with respect to the perpendicular easy axis.

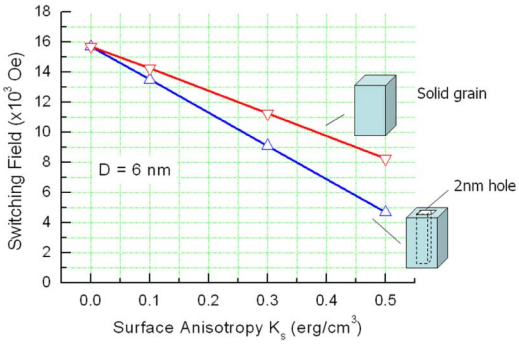

Fig. 16. Calculated switching field reduction as a function of surface anisotropy for a grain with a whole in the middle. The case without the whole is also plotted in comparison.

the presence of surface anisotropy. Fig. 16 shows the calculated switching field reductions as a function of surface anisotropy for a grain with a cylindrical hole through the entiregrain height. If surface anisotropy strength is significant, grains with a void or hole will certainly have significantly smaller switching field than that of a solid grain.

The presence of either round or slotted shaped cavities shown in the transmission electron microscopy analysis presented in previous section also results in an increase of inside surface area compared with the same size solid grains.

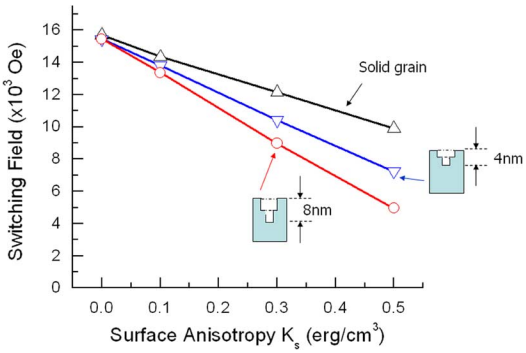

Fig. 17. Calculated switching field as a function of surface anisotropy strength for a solid grain (black), a grain with a 4 nm deep cavity (blue), and a grain with 8-nm-deep cavity. The diameter of the grains is $D = 8$ nm.

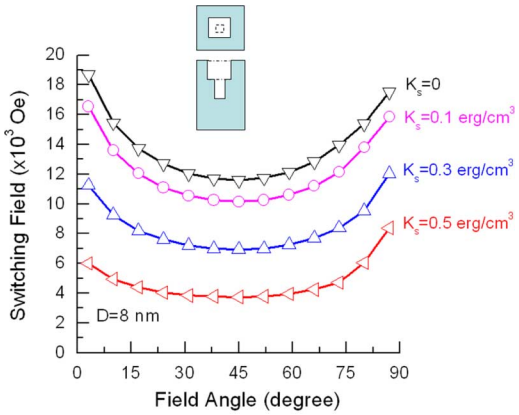

Fig. 18. Calculated switching field as a function of applied field angle for a grain with a cavity in the middle of the grain at the top. The depth of the cavity is 8 nm. Results for four different values of the surface anisotropy energy constant are shown.

Fig. 17 shows calculated switching field as a function of surface anisotropy strength. The switching field reduction becomes greater if the depth of the cavity is deeper.

Fig. 18 shows calculated switching field angle dependence for a grain with 8 nm deep cavity at various surface anisotropy strengths. In the presence of significant surface anisotropy, a cavity at top of the grain causes significant local reduction of the effective perpendicular anisotropy, consequently yielding nonuniform magnetization switching and resulting in a change of field angular dependence.

IV. Summary and Remarks

A systematic transmission electron microscopy analysis, combining EELS elemental mapping and HAADF imaging technique, has been performed on current perpendicular granular/oxide thin-film media. In particular, the study focuses on the granular magnetic layer with oxide grain boundaries. It is found that the magnetic grains exhibit structure somewhat similar to the growth of a tooth, forming round and slot shaped cavities in the grains. Such topography is responsible for causing the apparent composition variation within the grains. It is also found that for CoCrPt-TiOx media, pronounced Cr segregation to the grain boundaries and also the cavities has been observed. Such elemental segregation is much less obvious in CoCrPt-SiOx media. Little oxide is observed inside the cavities for the studied medium samples with either type of oxide.

The cavity-present grain topography alone will only result in a reduction of grain volume and may not cause significant impact to recording density capability. However, in the presence of possible surface magnetic anisotropy that has easy axis normal to the surface, the cavity presence may yield a significant switching field reduction due to the surface area increase, especially for small grain sizes. Since the surface anisotropy arises from the electron wave function asymmetry at the interface, atomic composition and structure at grain boundary interface could be crucial for achieving high effective perpendicular anisotropy [15].

Acknowledgment

The authors would like to thank V. Sokalski and Dr. G. A. Prinz for many helpful discussions on grain growth and surface anisotropy. This work was supported in part by the Data Storage Systems Center at Carnegie Mellon University, Showa Denko K.K.K., and Williams Advanced Materials.

References

[1] K.-Z. Gao and H. N. Bertram, "Transition jitter estimations in tilted and conventional perpendicular recording media at 1 Tb/in," *IEEE Trans. Magn.*, vol. 39, no. 2, pp. 704–709, Mar. 2003.

[2] J.-G. Zhu, Y. Peng, and D. E. Laughlin, "Towards an understanding of grain-to-grain anisotropy field variation in thin film media," *IEEE Trans. Magn.*, vol. 41, p. 543, 2005.

[3] Y. Shimizu and H. N. Bertram, "Micromagnetic study of the transition parameter and position jitter in perpendicular recording," *IEEE Trans. Magn.*, vol. 39, no. 3, pp. 1846–1850, May 2003.

[4] M. Mochizuki, M. Hara, A. Nakamura, and M. Igarashi, "Write-field gradient effect on transition width in perpendicular recording media," *IEEE Trans. Magn.*, vol. 41, no. 10, pp. 3082–3084, Oct. 2005.

[5] N. C. Koon, B. T. Jonker, F. A. Volkening, J. J. Krebs, and G. A. Prinz, "Direct evidence for perpendicular spin orientations and enhanced hyperfine fields in ultrathin Fe(100) films on Ag(100)," *Phys. Rev. Lett.*, vol. 59, p. 2463, 1987.

[6] H. Fritzsche, J. Kohlhepp, and U. Gradmann, "Second- and fourth-order magnetic surface anisotropy of Co(0001)-based interfaces," *J. Magn. Magn. Mater.*, vol. 148, pp. 154–155, 1995.

[7] Y. Sonobe, D. Weller, Y. Ikeda, K. Takano, M. E. Schabes, G. Zeltzer, H. Do, B. K. Yen, and M. E. Best, "Coupled granular/continuous medium for thermally stable perpendicular magnetic recording," *J. Magn. Magn. Mater.*, vol. 235, pp. 424–428, 2001.

[8] H. Muraoka, Y. Sonobe, K. Miura, A. M. Goodman, and Y. Nakamura, "Analysis on magnetization transition of CGC perpendicular media," *IEEE Trans. Magn.*, vol. 38, pp. 1632–1636, 2002.

[9] A. M. Goodman, S. J. Greaves, Y. Sonobe, H. Muraoka, and Y. Nakamura, "Smoothing of bit transition irregularity in CGC perpendicular media," *J. Appl. Phys.*, vol. 91, p. 8064, 2002.

[10] A. M. Goodman, S. J. Greaves, Y. Sonobe, H. Muraoka, and Y. Nakamura, "Simulations of magnetic recording in coupled granular/continuous perpendicular media with random pinning sites," *IEEE Trans. Magn.*, vol. 38, pp. 2051–2053, 2001.

[11] A. J. Gubbens and O. L. Krivanek, *Ultramicroscopy*, vol. 51, p. 146, 1993.

[12] J. D. Risner *et al.*, "Analytical transmission electron microscopy examinations of CoPt-TiO_2 perpendicular magnetic recording media," *Microsc. Microanal.*, vol. 13, pp. 70–79, 2007.

[13] J. Bentley, J. D. Risner, and R. Sinclair, "Composition mapping of Co-Pt-Ti-O perpendicular magnetic recording media by simultaneous EDS and EELS spectrum imaging," *Microsc. Microanal.*, vol. 13, 2007.

[14] J. D. Risner, "High Resolution Analytical Transmission Electron Microscopy of Magnetic Recording Media," Ph.D. dissertation, Material Science and Engineering, Stanford University, Stanford, CA, Mar. 2006.

[15] F. Luis *et al.*, "Tuning the magnetic anisotropy of Co nanoparticles by metal capping," *Europhys. Lett.*, vol. 76, pp. 142–148, 2006.